WAVY TAYLOR VORTICES IN PLANE COUETTE FLOW*

A. J. CONLEY† AND H. B. KELLER‡

Abstract. Path-following techniques applied to a spectral approximation of the solution of the Navier-Stokes Equations have revealed the existence of a new class of solutions to the plane Couette flow problem.

Key words. Path Following, Plane Couette Flow, Bifurcation, Navier-Stokes Equations, Taylor–Couette Flow

AMS subject classifications. 35-04, 35B30, 35B32, 35B60, 35Q30, 65N35, 76-04, 76D05, 76D33, 76E05, 76E30.

1. Introduction. A long-standing problem in fluid mechanics is understanding the transitions from laminar to turbulent flow. This problem has been studied in many specific cases. Plane Couette flow, the case of interest in this paper, is the flow of an incompressible viscous fluid between infinite parallel shearing plates.

Experimentally, plane Couette flow sustains turbulence for large enough Reynolds number ($Re > Re_t = 1440 \pm 40$) (see [7]). For Reynolds numbers less than the transition number ($Re < Re_t$) the flow becomes a laminar flow with the velocity depending only on the distance from each plate. Theoretically and numerically, all studies seem to imply linear stability of this laminar flow for all Reynolds numbers (see [6] [1]). The lack of bifurcations or other known solutions for plane Couette flow make the study of this transition difficult.

In contrast, Taylor–Couette flow, the flow between infinitely long coaxial cylinders, bifurcates to other flows for large enough Reynolds numbers. If the gap between the cylinders is small compared with the average radius of the cylinders, Taylor–Couette flow is approximated by plane Couette flow in a tumbling channel. This limit is discussed in Appendix A.

New solutions of the plane Couette flow problem have recently been found (see [3],[4],[5]) by studying plane Couette flow in a channel tumbling with speed Ω about the z axis (see Fig. (1.1)). By varying the tumbling rate, bifurcations from one- to two-dimensional solutions and subsequent bifurcations from two- to three-dimensional solutions are found. The two–dimensional solutions look like Taylor vortices in Taylor–Couette flow. The axis of each vortex is aligned with the velocity of the bounding plates. The three–dimensional solutions bifurcating from the vortex solution look like wavy Taylor vortices in Taylor–Couette flow. The tumbling rate, Ω, can be decreased to zero while retaining the three–dimensional structure of the solutions.

The use of Chebyshev polynomials and the path following techniques of H. B. Keller [2] provide better-resolved solutions and make it possible to find the minimum Reynolds number at which these solutions exist. This minimum Reynolds number ($Re = 470$) is about one third the Reynolds number at which the flow experimentally sustains turbulence. Linear stability analysis of this flow implies that the solutions are probably unstable.

Formulation. Define

$$\vec{U}(x,y,z) = \begin{pmatrix} u(x,y,z) \\ v(x,y,z) \\ w(x,y,z) \end{pmatrix}$$

to be the velocity of the flow at location (x,y,z) (see Fig. (1.1)). Define $p(x,y,z)$ to be the pressure of the flow. The Navier–Stokes equations for traveling wave solutions between parallel plates rotating

* This research was supported in part by the National Science Foundation under Cooperative Agreement No. CCR-9120008, in part by the Office of Scientific Computing, U.S. Department of Energy, under Contract W-31-109-Eng-38, and in part by the U.S. Department of Energy under Grant No. DE-FG03-89ER25063.

† Mathematics and Computer Science Division, Argonne National Laboratory, Argonne, IL 60439.

‡ Applied Mathematics, California Institute of Technology 217-50, Pasadena, CA 91125.

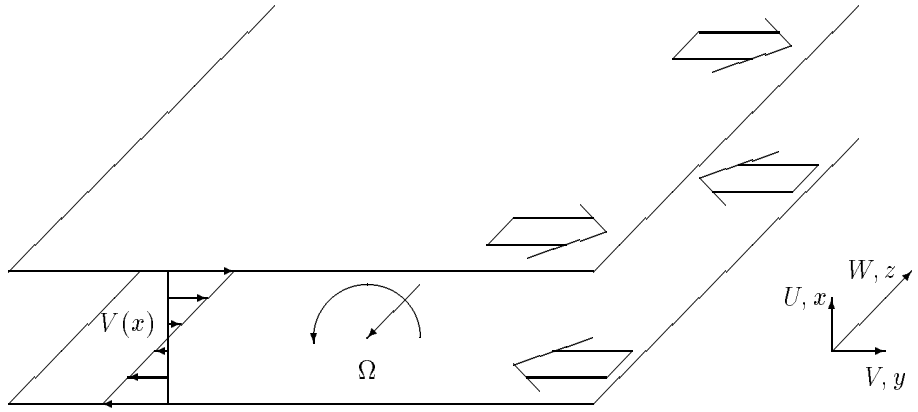

FIG. 1.1. *We study flow between infinite parallel shearing plates. The plates are tumbling with angular velocity, Ω. The linear velocity profile, $V(x)$, is stable for all shear rates.*

about an axis parallel to the z-axis with speed Ω are

$$0 = -\,\mathrm{Re}\,(\vec{U}\cdot\vec{\nabla})\vec{U} + \nabla^2\vec{U} - \vec{\nabla}p + 2\Omega(\hat{z}\times\vec{U}) + c_y\partial_y\vec{U} + c_z\partial_z\vec{U}, \tag{1.1}$$

$$0 = \vec{\nabla}\cdot\vec{U}. \tag{1.2}$$

Here, $\hat{z}$, is the unit vector in the z direction, and c_y and c_z are the wave speeds of the flow in the y and z directions, respectively. The nondimensional Reynolds number, Re, is the velocity difference of the plates times the distance of the gap between the plates divided by the viscosity. (The wave speeds of all solutions in this paper are found to be zero.) The solutions of these equations are required to satisfy no-slip boundary conditions at the plates, which move with speeds $\pm 1/2$. Periodic boundary conditions are imposed in the y and z directions, parallel to the plates. With unit vector $\hat{y}$ in the y direction and periods λ_y and λ_z in the y and z directions, respectively, these boundary conditions are

$$\vec{U}(-\frac{1}{2},y,z) = +\frac{1}{2}\hat{y}, \tag{1.3}$$

$$\vec{U}(\frac{1}{2},y,z) = -\frac{1}{2}\hat{y}, \tag{1.4}$$

$$\vec{U}(x,y+\lambda_y,z) = \vec{U}(x,y,z), \tag{1.5}$$

$$p(x,y+\lambda_y,z) = p(x,y,z), \tag{1.6}$$

$$\vec{U}(x,y,z+\lambda_z) = \vec{U}(x,y,z), \tag{1.7}$$

$$p(x,y,z+\lambda_z) = p(x,y,z). \tag{1.8}$$

The shear force at the lower plate,

$$\tau(\vec{U}) = -\frac{1}{\lambda_y\lambda_z}\int_0^{\lambda_y} dy \int_0^{\lambda_z} dz \frac{\partial v}{\partial x}(-1/2,y,z), \tag{1.9}$$

is used as a parameter of the solution in the continuation procedures.

The well-known Couette flow,

$$\vec{U}(x,y,z) = \begin{pmatrix} 0 \\ -x \\ 0 \end{pmatrix}, \tag{1.10}$$

$$p = -\Omega x^2,$$

satisfies these equations for all $Re, \lambda_y, \lambda_z, c_y$, and c_z. This paper is concerned with paths of solutions that bifurcate from this branch of solutions.

Section 2 describe the solution approximation scheme. Section 3 describes the methods used to follow paths of solutions and to switch branches of solutions. Additional phase constraints (which are necessary because of the periodic boundary conditions) are also described. Sections 4 and 5 describe the solutions and their linear stability.

2. Approximation of Velocity and Pressure Fields. The solutions are expanded in terms of

$$C_{l,m,n}(x,y,z) = T_l(2x)\cos(m\alpha_y y + n\alpha_z z),$$

$$S_{l,m,n}(x,y,z) = T_l(2x)\sin(m\alpha_y y + n\alpha_z z),$$

$$A_{l,m,n} = (C_{l,m,n} + iS_{l,m,n}) = T_l(2x)e^{i(m\alpha_y y + n\alpha_z z)}.$$

Here, $\alpha_y = \frac{2\pi}{\lambda_y}$, and $\alpha_z = \frac{2\pi}{\lambda_z}$ are the y and z wave numbers, respectively. Each of u, v, w, and p are approximated by finite expansions of the form

$$q(x,y,z) = \sum_{l=0}^{L}\sum_{m=-M}^{M}\sum_{n=-N}^{N} q_{l,m,n}A_{l,m,n}(x,y,z).$$

Here, q represents u, v, w, or p. As a result, the approximated $\vec{U}$ and p are determined by a total of $4(L+1)(2M+1)(2N+1)$ coefficients. The same notation for the approximations and the solutions is used in this paper.

These approximations do not (in general) satisfy the Navier–Stokes equations. As a result, only certain projections of the Navier–Stokes equations are required to be zero. Define the inner products,

$$< A_{lmn}, f > = \int_{1/2}^{1/2} \frac{dx}{\sqrt{1-4x^2}} \int_0^{\lambda_y} dy \int_0^{\lambda_z} dz (A_{lmn} \cdot f), \tag{2.1}$$

$$\langle e^{i(m\alpha_y y + n\alpha_z z)}, f\rangle = \int_0^{\lambda_y} dy \int_0^{\lambda_z} dz (e^{i(m\alpha_y y + n\alpha_z z)} f). \tag{2.2}$$

Define $\vec{M}$ to be the right-hand side of Eq. (1.1). Then the $4(L+1)(2M+1)(2N+1)$ equations that the approximations are required to satisfy are the following:

$$< A_{lmn}, \vec{M} > = 0 \begin{cases} 0 \le l \le L-2, \\ |m| \le M, \\ |n| \le N \end{cases} \tag{2.3}$$

$$< A_{lmn}, \vec{\nabla} \cdot \vec{U} > = 0 \begin{cases} 0 \le l \le L-2, \\ |m| \le M, \\ |n| \le N \end{cases} \tag{2.4}$$

$$\langle e^{i(m\alpha_y y + n\alpha_z z)}, \vec{U}(\pm 1/2, y, z) \pm 1/2\hat{y}\rangle = 0 \begin{cases} |m| \le M, \\ |n| \le N. \end{cases} \tag{2.5}$$

In addition, since the periodicity in y and z introduces a two-dimensional nonuniqueness, the following two phase constraints are imposed on the solutions:

$$< C_{001}, u(x,y,z) >= 0, \tag{2.6}$$

$$< S_{010}, w(x,y,z) >= 0. \tag{2.7}$$

Equations (2.3)–(2.5) are referred to as

$$F(u,\lambda) = 0$$

in the rest of this paper. The solution u is the set of coefficients that determine $\vec{U}$ and p. The parameter λ is typically Ω, Re, α_y, or α_z. Both of the phase constraints are trivially satisfied on the Couette flow branch of solutions. Phase constraint (2.6) is imposed on the vortex branch, and both phase constraints are imposed on the wavy vortex branch. When the phase constraints are imposed, they are adjoined to $F(u,\lambda)$. As a result, additional quantities are necessary. Hence, the wave speeds c_y and c_z are introduced and solved for u (in addition to the coefficients).

3. Path Following. Continuation methods are used to approximate the solution path

$$\Gamma = \{(u,\lambda) : F(u,\lambda) = 0\}.$$

Three distinct methods are employed, depending on the presence of folds or bifurcations. In the case of regular path segments the algorithm used is as follows:

Step 1. Start with an initial solution, (u_0, λ_0). Construct the Jacobian

$$F_u^0 = \frac{\partial F(u_0;\lambda_0)}{\partial u}.$$

Step 2. Construct the initial iterate and initial parameter with one of the following:

- constant value continuation: $\lambda_i = \lambda_{i-1} + \delta\lambda, u_i^0 = u_{i-1}$
- secant continuation: $\lambda_i = \lambda_{i-1} + \delta\lambda$, $u_i^0 = u_{i-1} + \frac{\lambda_i - \lambda_{i-1}}{\lambda_{i-1} - \lambda_{i-2}}(u_{i-1} - u_{i-2})$.

Step 3. Compute the special Newton iterates (indexed by $\nu = 1, 2, ...$),

$$F_u^0 \epsilon^\nu = -F(u_i^\nu; \lambda_i),$$

$$u_i^{\nu+1} = u_i^\nu + \epsilon_i^\nu,$$

until $||\epsilon_i^N||_{l_1} < \epsilon$.

Step 4. Set $u_i = u_i^{N+1}$. If the parameter λ_i is still in the desired range, and the number of iterations is small ($N < 30$), return to Step 2.

This algorithm may fail for several reasons. One is that the step $\delta\lambda$ is too large. In this case, decrease the step size. Another reason the algorithm may fail is that the iterates in step 3 converge too slowly. In this case, recompute the Jacobian. Lastly, the solution path may trespass a bifurcation point or may step beyond the solution path at a fold. In this case, use one of the following algorithms for folds or bifurcations.

At a fold point the Jacobian is singular. Thus, as it is approached, the shear force (1.9) at the lower plate is introduced as a new parameter. (In Taylor–Couette flow, τ corresponds to the torque on the inner cylinder.) To continue the solution past the fold, adjoin the equation

$$\tau(u) = \tau_i, \tag{3.1}$$

and seek solutions of the expanded system:

$$G(u(\tau_i), \lambda(\tau_i); \tau_i) = \begin{pmatrix} F(u(\tau_i), \lambda(\tau_i)) \\ \tau(u(\tau_i)) - \tau_i \end{pmatrix} = 0. \tag{3.2}$$

By varying τ_i, a path of the form

$$\hat{\Gamma} = \{(u(\tau_i), \lambda(\tau_i), \tau_i) : G(u,\lambda,\tau) = 0, \tau_a < \tau_i < \tau_b\}$$

is generated. This leads to the following algorithm for finding a segment of the path near a fold:

Step 1. Start with an initial solution, (u_0, λ_0). Construct the Jacobian

$$G_x^0 = [G_u^0 : G_\lambda^0] = \begin{bmatrix} F_u^0 & F_\lambda^0 \\ \tau_u & 0 \end{bmatrix}.$$

Step 2. Construct the initial iterate and new parameter with one of the following:

- constant value continuation: $\tau_i = \tau_{i-1} + \delta\tau, u_i^0 = u_{i-1}, \lambda_i^0 = \lambda_{i-1}$
- secant continuation:

$$\tau_i = \tau_{i-1} + \delta\tau,$$

$$u_i^0 = u_{i-1} + \frac{\tau_i - \tau_{i-1}}{\tau_{i-1} - \tau_{i-2}}(u_{i-1} - u_{i-2}),$$

$$\lambda_i^0 = \lambda_{i-1} + \frac{\tau_i - \tau_{i-1}}{\tau_{i-1} - \tau_{i-2}}(\lambda_{i-1} - \lambda_{i-2}).$$

Step 3. Compute the special Newton iterates (indexed by $\nu = 1, 2, ...$),

$$G_x^0 \begin{pmatrix} \epsilon_i^\nu \\ l_i^\nu \end{pmatrix} = \begin{pmatrix} -F(u_i^\nu; \lambda_i^\nu) \\ -\tau(u_i^\nu) + \tau_i \end{pmatrix},$$

$$u_i^{\nu+1} = u_i^\nu + \epsilon_i^\nu,$$

$$\lambda_i^{\nu+1} = \lambda_i^\nu + l_i^\nu,$$

until $||\epsilon_i^N||_{l_1} + |l_i^N| < \epsilon$.

Step 4. Set $u_i = u_i^{N+1}, \lambda_i = \lambda_i^{N+1}$. If τ_i is still in the desired range, and the number of iterations N is small, return to Step 2.

When the iterations in step 3 fail to converge, return to continuation in λ.

To switch from Couette flow (1.10) to the vortex solution, first locate the critical Ω at which the Jacobian is singular ($Re = 600, \Omega_c = 1.43, \alpha_z = 3.1163$). Since the Navier–Stokes equations are autonomous in z and the solution is to be periodic in z, it follows that the Jacobian has a two-dimensional null space. Thus two constraints can be imposed. One is the phase constraint (2.6), which can be rewritten as

$$\Phi_z(u) = \int_{-\frac{1}{2}}^{\frac{1}{2}} \frac{dx}{\sqrt{1-4x^2}} \int_0^{\lambda_y} dy \int_0^{\lambda_z} dz \cos(2\pi z/\lambda_z) u(x, y, z) = 0. \tag{3.3}$$

The other constraint requires the solution to have a constant component in the direction of the null vector of the Jacobian F_u. Because two new constraints have been imposed, the two parameters Ω and c_z are freed. To solve this augmented system, we use a new algorithm:

Step 1. Accurately find the parameter value λ^* at which

$$F_u^* = \frac{\partial F(u(\lambda^*), \lambda^*)}{\partial u}$$

is singular.

Step 2. Find the right null vector, ϕ, of the singular Jacobian with $\Phi_z(\phi) = 0$.

Step 3. Construct an initial guess for a solution on the new branch, $u_i^o = u(\lambda^*) + \epsilon\phi$.

Step 4. Compute the Newton iterates for the augmented system,

$$\begin{pmatrix} F(u, c_z, \lambda) \\ \phi \cdot u \\ \Phi_z(u) \end{pmatrix} = \begin{pmatrix} 0 \\ \phi \cdot u_i^0 \\ 0 \end{pmatrix}.$$

Here, an additional constraint,

$$\Phi_y(u) = \int_{-\frac{1}{2}}^{\frac{1}{2}} \frac{dx}{\sqrt{1-4x^2}} \int_0^{\lambda_y} dy \int_0^{\lambda_z} dz \sin(2\pi y/\lambda_y) w(x, y, z) = 0, \tag{3.4}$$

has been adjoined, and the parameter c_z has been freed as a variable. To compute solutions along the vortex branch, use the algorithm to find the segment of the path near a fold or use the algorithm for a regular path but use the augmented system of equations,

$$H(u, c_z, \lambda) = \begin{pmatrix} F(u, c_z, \lambda) \\ \Phi_z(u) \end{pmatrix} = 0,$$

instead of $F(u, \lambda) = 0$. Finally, to switch paths from vortex to wavy vortex solutions, use the following algorithm:

Step 1. Accurately find the parameter value λ^* at which the Jacobian

$$(H_u(u(\lambda^*), c_z, \lambda^*) | H_{c_z}(u(\lambda^*), c_z, \lambda^*))$$

is singular.

Step 2. Find the right null vector, ϕ, of the singular Jacobian with $\Phi_y(\phi) = 0$.

Step 3. Construct an initial guess for a solution on the new branch, $u_i^o = u(\lambda^*) + \epsilon\phi$.

Step 4. Compute the Newton iterates on the fully augmented system,

$$\begin{pmatrix} F(u, c_y, c_z, \lambda) \\ \phi \cdot u \\ \Phi_z(u) \\ \Phi_y(u) \end{pmatrix} = \begin{pmatrix} 0 \\ \phi \cdot u_i^0 \\ 0 \\ 0 \end{pmatrix}.$$

To compute solutions along the wavy vortex branch, use the algorithm for the path segments on a regular path or near a fold with the system

$$I(u, c_y, c_z, \lambda) = \begin{pmatrix} F(u, c_y, c_z, \lambda) \\ \Phi_z(u) \\ \Phi_y(u) \end{pmatrix} = 0,$$

instead of $F(u, \lambda) = 0$.

4. Couette Flow to Vortices. At $Re = 600, \Omega_c = 1.43, \alpha_z = 3.1163$, the paths of Couette flow and vortex flow intersect. The analysis in Appendix B shows that the locations of the bifurcations from the Couette solutions are a function of the Taylor number

$$T = 2\Omega(Re - 2\Omega)$$

and the wave number α_z. The locations of these bifurcation points are not independent functions of the Reynolds number and Ω. The Taylor number at which the Jacobian is singular is called the critical Taylor number, T_c.

Note that the Taylor number is quadratic in Ω. Thus, for large enough Reynolds numbers,

$$Re > 2\sqrt{T_c},$$

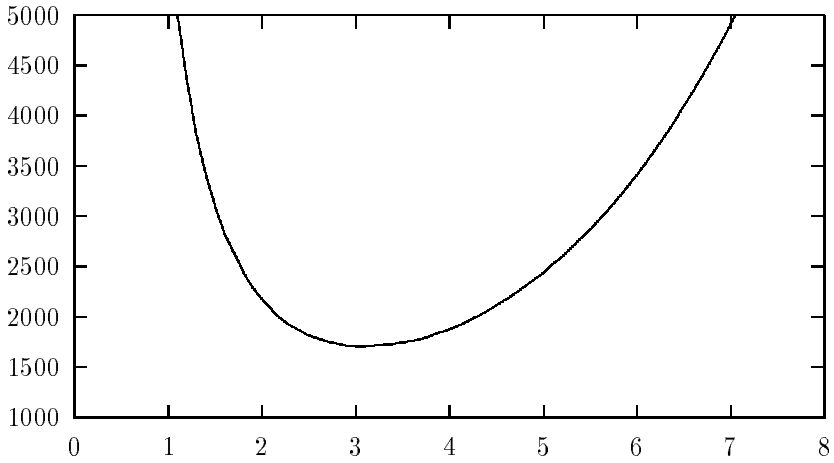

FIG. 4.1. *T_c vs α_z*

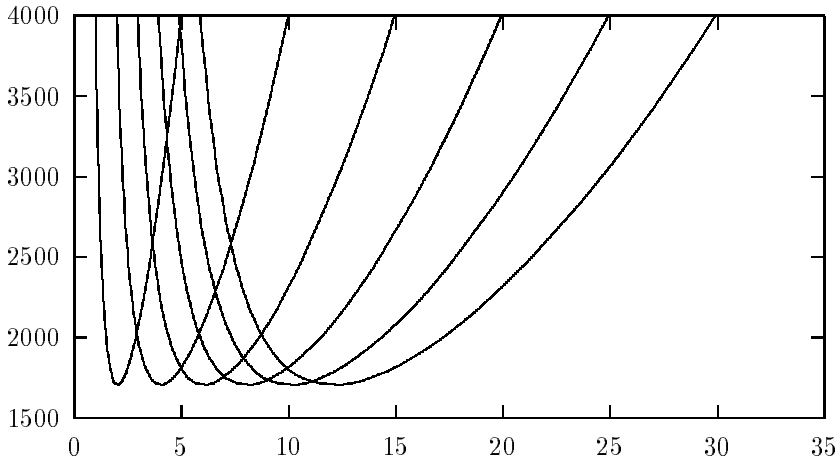

FIG. 4.2. *T_c vs λ_z when the x-direction is spanned by 33 Chebyshev polynomials*

there are at least two singular points. In the generic case, there are an even number of singular points.

T_c varies with $\alpha_z = 2\pi/\lambda_z$; however, it does not vary with α_y. See Figure 4.1 for a graph of T_c as a function of α_z. Since the boundary conditions are periodic, if the Jacobian is singular at (T_c, λ_z) then the Jacobian is also singular for all periodicities that are integral multiples of $\lambda_{z,c}$, namely, $(T_c, n\lambda_z)$. Figure 4.2 is a graph of the critical Taylor number against the periodicity λ_z. Only the first six multiples of the fundamental mode are shown.

To compute these values of the critical Taylor number, fix the Reynolds number at $Re = 600$. At different values of the wave number, α_z, increase Ω from zero (in steps of .05). Determine the

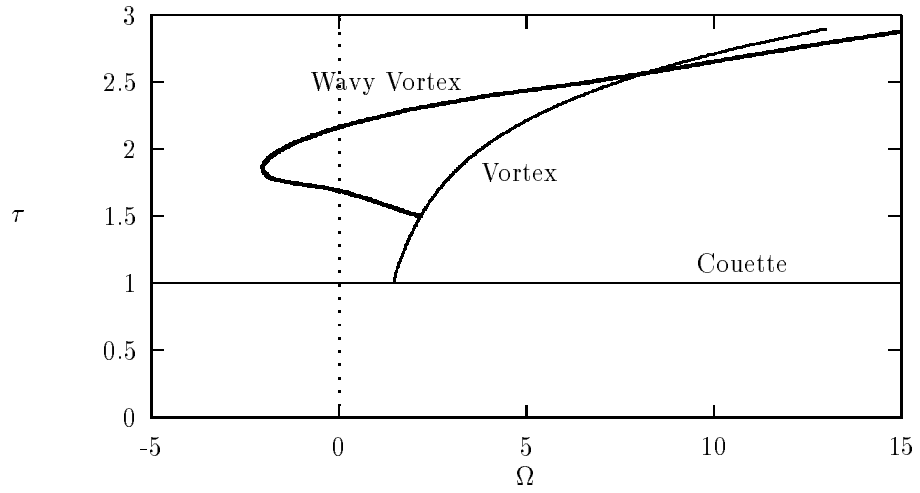

FIG. 4.3. *Shear stress as a function of* Ω. $Re = 600, \alpha_y = 1.6, \alpha_z = 3.0$. *The lower intersection of vortex and wavy vortex branches is a bifurcation. The upper intersection of the vortex and wavy vortex branches is only graphical. (The flows are not the same at this point.) There are two wavy vortex solutions at* $\Omega = 0$. *The solution with large shear stress is called the upper branch solution, and that with low shear stress is called the lower branch solution. The resolution is* $(L, M, N) = (14, 3, 3)$ *in this picture.*

value of Ω at which the Jacobian has the smallest (magnitude) determinant. Then compute the Taylor number using $T = 2\Omega(Re - 2\Omega)$. Compute the critical Taylor number for different values of the wave number α_z. This gives the function $T_c(\alpha_z)$. Lastly, compute Newton iterations on the minimum problem,

$$\frac{\partial T_c}{\partial \alpha_z} = 0,$$

to find the minimum critical Taylor number,

$$T_{c,min} = 1707.7618$$

when the wave number is

$$\alpha_z = 3.1163/n.$$

At the bifurcation point, switch to the new branch of solutions (the vortex branch by the methods discussed in Section 2). While the Couette solution has a constant shear force of 1.0 for all values of Ω, the new branch of solutions (labeled "Vortex" in Figure 4.3) increases in shear force with increasing Ω.

These vortices have some symmetries. The solution branch varies only with x and z. There is no y variation. A graph of the mean flow in the y direction is shown in Figure 4.4, and the flow perpendicular to y is shown in Figure 4.5.

Follow the vortex solution from $\Omega = 1.43$ where it bifurcates from Couette flow to $\Omega = 13$. (See Fig. 4.3.) During this continuation the Jacobian is singular at $\Omega = 2.1725$, signaling a secondary bifurcation. The new branch (labeled "Wavy Vortex" in Fig. 4.3) of solutions bifurcating from the vortex branch is discussed in Section 5.

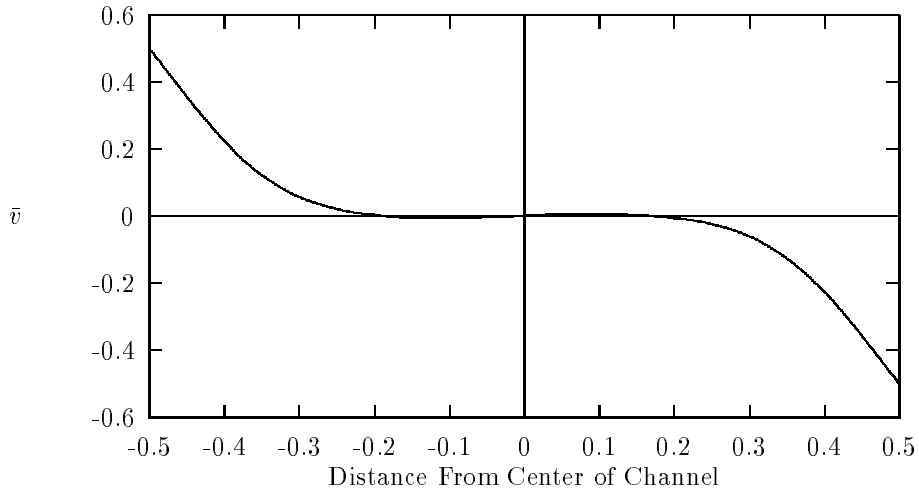

FIG. 4.4. *The mean (over a period in y and z) of the flow in the y direction for the vortex solution at Re=600,* $\Omega = 13$, $\alpha_z = 3.0$.

FIG. 4.5. *The velocity field in the xz plane for the vortex solution at Re=600,* $\Omega = 13$, $\alpha_z = 3.0$. *The lower plate is shearing out of the paper on the lower edge of the image.*

At lower Reynolds numbers (i.e., $Re < 250$), the full path of vortex solutions can be computed. At wave number $\alpha_z = 3.0$, the critical Taylor number is $T_c = 1711.28$. Thus, at Reynolds number 85.0, the two values of Ω that satisfy the equation

$$T_c = 2\Omega(Re - 2\Omega)$$

are $\Omega = 16.377$ and $\Omega = 26.123$. As can be seen in Fig. 4.6, one vortex solution branch intersects the Couette flow branch at these two points.

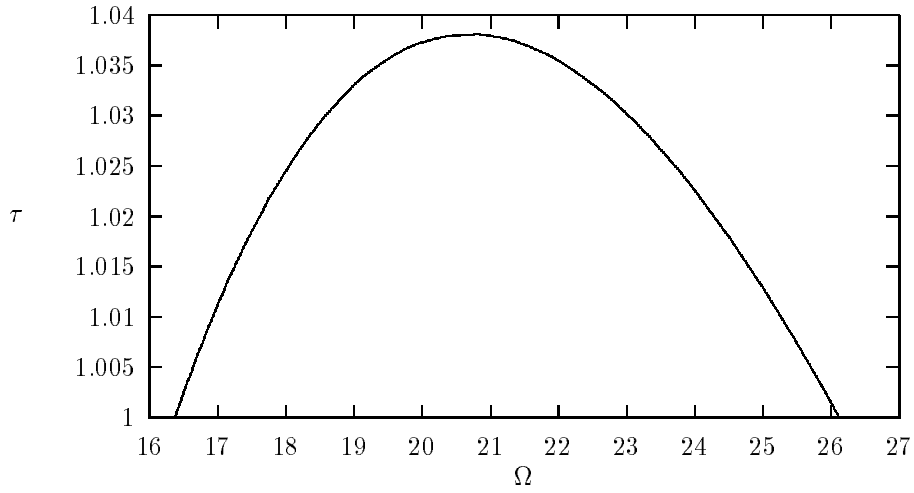

FIG. 4.6. *Shear stress vs.* Ω *at* $Re = 85.0, \alpha_z = 3.0, \alpha_y = 1.6$. *This branch of vortices shows that the two values of* Ω *satisfying* $2\Omega(Re - 2\Omega) = T_c$ *correspond to bifurcation points on the same branch of vortex solutions.*

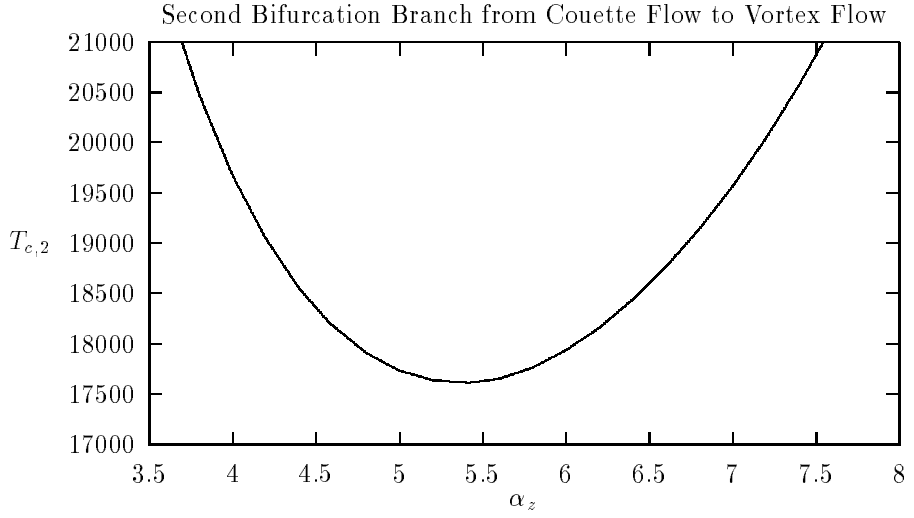

FIG. 4.7. *Couette flow bifurcates to a different path of solutions at higher Taylor number. This second branch of critical Taylor numbers has a minimum near 17700 when* α_z *is near 5.4.*

At the same wave number, $\alpha_z = 3.0$, there is a sequence of critical Taylor numbers, say, $T_{c,\nu}, \nu = 1, 2, ...$, that satisfy Eq. (B.4). The next two values of the critical Taylor number are $T_{c,2} \doteq 26,100$ and $T_{c,3} \doteq 182,300$. These critical Taylor numbers also vary with α_z. Figure 4.7 shows the relation between $T_{c,2}$ and the wave number, α_z. Note that the minimum value of $T_{c,2}$ is nearly ten times the minimum value of $T_{c,1}$ (graphed in Fig. 4.1 and labeled T_c.)

5. Vortices to Wavy Vortices. On the vortex solution branch bifurcating from Couette flow, the Jacobian is singular at parameter values $Re = 600, \Omega = 2.17, \alpha_y = 1.6, \alpha_z = 3.0$. The

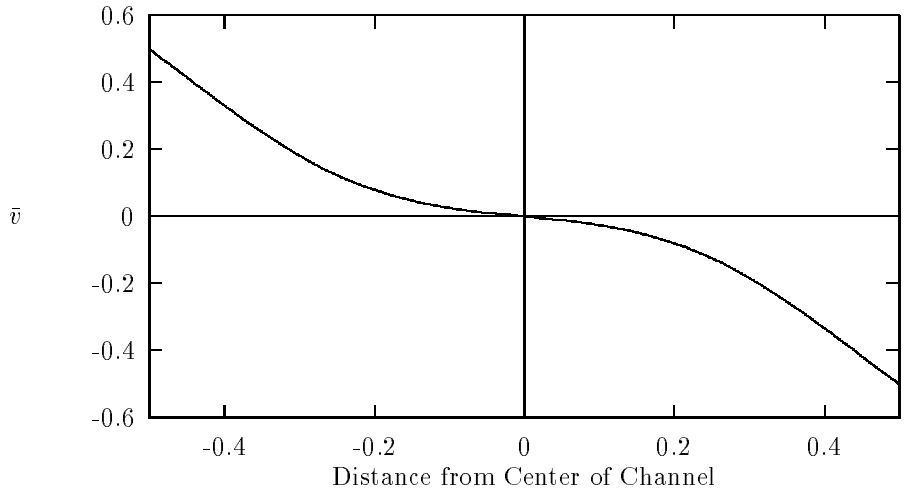

FIG. 5.1. *The mean flow in the y direction of the lower branch solution as a function of distance from center of channel.* $Re = 600, \alpha_y = 1.6, \alpha_z = 3.0, \Omega = 0, \tau = 1.7$.

TABLE 5.1
The lower branch wavy vortex solution (at $\Omega = 0$*) is resolved well enough that the shear stress of the solution at the lower plate has a relative error of less than 4%.*

Resolution L,M,N	Shear Stress at Lower Plate
13,3,3	1.72177413
14,3,3	1.69405548
15,3,3	1.70084151
16,3,3	1.69987208
17,3,3	1.69936109
18,3,3	1.69959818
14,3,4	1.68283399
14,3,5	1.66029900
14,4,4	1.66777241
14,4,5	1.67317174

new path of solutions is labeled "Wavy Vortex" in Fig. 4.3. Note that the path has a fold point ($\tau = 1.86, \Omega = -2.07$) and two solutions at $\Omega = 0$. Call the solution (at $\Omega = 0$) with larger shear stress the upper branch solution and the solution with smaller shear stress the lower branch solution. Table 5.1 indicates that there is a relative error of less than 4% in the shear stress for resolutions above $(L, M, N) = (13, 3, 3)$.

Figure 5.1 shows the mean velocity in the y direction for comparison with the vortex solution (Figure 4.4). Figure 5.2 shows the x-z cross sections of the velocity field for different values of y. Compare the vortex solution in Figure 4.5.

5.1. Minimum Reynolds Numbers. The two solutions at $\Omega = 0$ are functions of τ, α_y, α_z, and Re. To find the values of these parameters at which the Reynolds number is a minimum, let

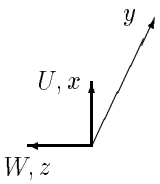

FIG. 5.2. *Cross sections (at* $y = 0, \frac{2\pi}{5}, \frac{4\pi}{5}, \frac{6\pi}{5}, \frac{8\pi}{5}, 2\pi$*) of the velocity field of the lower branch wavy vortex solution in the xz plane. The left-bottom cross section is at* $y = 0$ *and the upper-right cross section is at* $y = 2\pi$*.* $Re = 600, \alpha_y = 1.6, \alpha_z = 3.0$*. The lower plate is shearing out of the paper at the bottom of each cross section.*

$Re = Re(\tau, \alpha_y, \alpha_z)$, and consider the problem

$$\begin{pmatrix} F(u(\tau_0, \alpha_y, \alpha_z), Re(\tau_0, \alpha_y, \alpha_z)) \\ \Omega \\ \tau(u) - \tau_0 \end{pmatrix} = 0. \tag{5.1}$$

Figure 5.3 shows the variation of Reynolds number with shear stress (for $\alpha_y = 1.6, \alpha_z = 3.0$). The path segment in Figure 5.3 includes the two solutions in Figure 4.3 at $\Omega = 0$. For these values of the wave numbers, the minimum Reynolds number is 520; however, lower Reynolds number flows occur at different wave numbers.

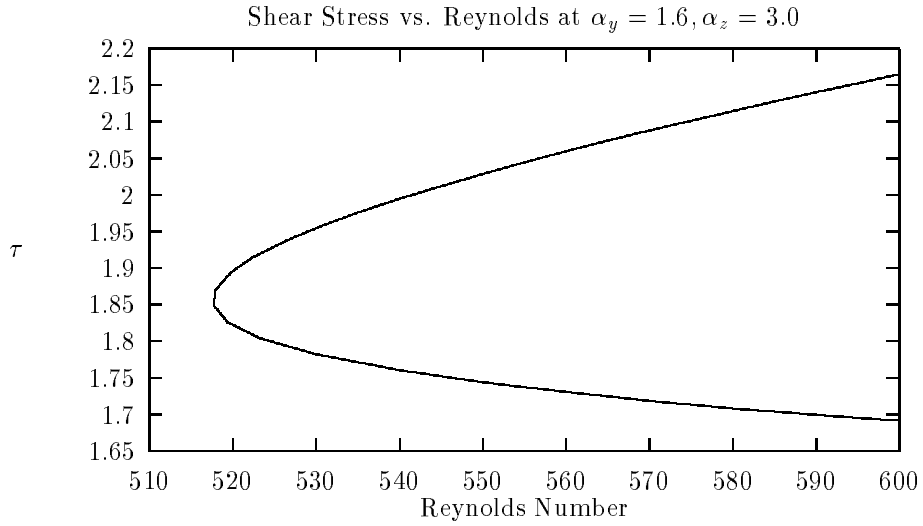

FIG. 5.3. *As the Reynolds number decreases from 600.0, the upper and lower branches of the $\Omega = 0$ wavy vortices coalesce and disappear.*

To find the (local) minimum Reynolds number for all wavenumbers and shear stresses, solve the minimum problem

$$\begin{pmatrix} \frac{\partial Re}{\partial \tau} \\ \frac{\partial Re}{\partial \alpha_y} \\ \frac{\partial Re}{\partial \alpha_z} \end{pmatrix} = 0 \tag{5.2}$$

by Newton's method. Start the Newton iterations with the solution at $\tau = 1.85, \alpha_y = 1.6, \alpha_z = 3.0$ in Figure 5.3. Each step of Newton's method requires 42 solutions of the Navier–Stokes equations in order to evaluate the finite-difference approximations of the derivatives appearing in the Newton iterations for this minimum problem. The minimum is found at the following values of the parameters:

$$\begin{aligned} Re &= 470, \\ \tau &= 1.70, \\ \alpha_y &= 0.96, \\ \alpha_z &= 2.00. \end{aligned}$$

These values are calculated with a resolution of $(L, M, N) = (14, 3, 3)$. The solution path (τ vs Ω) for these values of the Reynolds number and wave numbers is shown in Figure 5.4.

5.2. Linear Stability. The stability of the computed steady solution is determined by the usual linear stability analysis applied to the unsteady equations

$$\frac{\partial V}{\partial t} = -\ \mathrm{Re}\ (\vec{V} \cdot \vec{\nabla})\vec{V} + \nabla^2 \vec{V} - \vec{\nabla} p + 2\Omega(\hat{z} \times \vec{V}), \tag{5.3}$$

$$0 = \vec{\nabla} \cdot \vec{V}. \tag{5.4}$$

Here the time has been scaled by the square of the channel width and viscosity. This scaling leads to the eigenproblem

$$\lambda \vec{\epsilon} = -\ \mathrm{Re}\ [(\vec{V}_a \cdot \vec{\nabla})\vec{\epsilon} + (\vec{\epsilon} \cdot \vec{\nabla})\vec{V}_a] + \nabla^2 \vec{\epsilon} - \vec{\nabla} \rho + 2\Omega(\hat{z} \times \vec{\epsilon}) \tag{5.5}$$

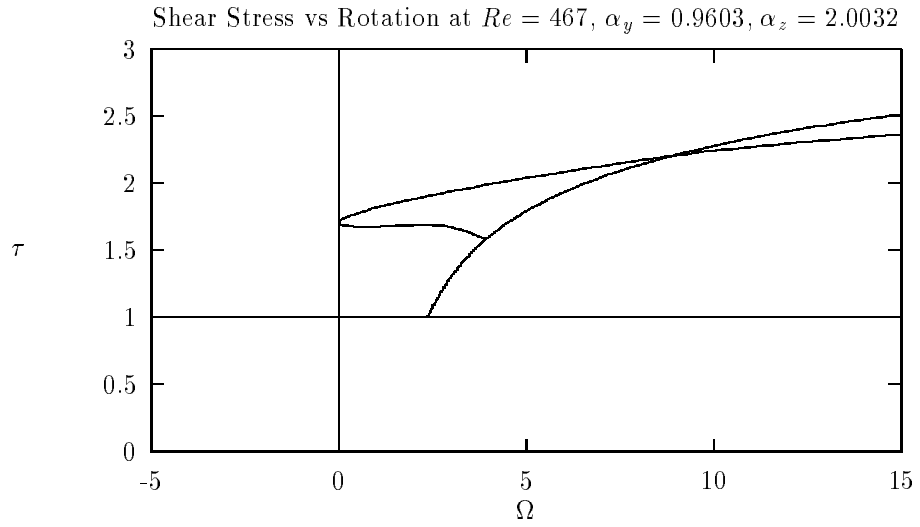

FIG. 5.4. *Solution path with resolution (L,M,N)=(14,3,3) at minimum Reynolds number Re=467.* $\alpha_y = .96$, $\alpha_z = 2.0$.

$$0 = \vec{\nabla} \cdot \vec{\epsilon}, \tag{5.6}$$

where $\vec{\epsilon}$ and ρ are the perturbations to $\vec{U}$ and p. They are approximated in the same way as $\vec{U}$ and p. Dirichlet boundary conditions at the x boundaries and periodic boundary conditions in y and z are applied. This process leads to a generalized eigenvalue problem of order 1454 (for $(L, M, N) = (14, 3, 3)$). There are some eigenvalues at infinity for generalized eigenvalue problems; however, numerical analysis (in finite precision) perturbs the eigenvalues at infinity to large eigenvalues. In particular, D projections of Eq. (5.5) and E projections of Eq. (5.6) lead to $D - E$ eigenvalues not "at infinity." At resolution $(L, M, N) = (14, 3, 3)$, there are 968 projections of Eq. (5.5) and 360 projections of Eq. (5.6). Thus, there are 588 meaningful eigenvalues and many meaningless large eigenvalues. Note that unstable modes correspond to eigenvalues with Real$(\lambda) > 0$ and stable modes correspond to eigenvalues with Real$(\lambda) < 0$. These eigenvalues are computed with EISPACK.

On the lower branch the parameters are $Re = 600, \alpha_y = 1.6, \alpha_z = 3.0, \Omega = 0$, and $\tau = 1.694$. Figure 5.5 shows the scattered eigenvalues of large magnitude. Figure 5.6 shows Figure 5.5 scaled by 100. There is a cluster of 588 eigenvalues near the origin. This cluster of eigenvalues is shown at much larger scale in Figure 5.7. Note that there is one eigenvalue in the right half plane, and hence the solution is unstable.

Figure 5.8 shows the eigenvalues of the upper branch solution. The pair of unstable eigenvalues suggests that there may have been a Hopf bifurcation on the path between the lower branch solution and the upper branch solution.

Lastly, at the minimum Reynolds number solution, the eigenvalues (Figure 5.9) are all in the left half plane except for the two eigenvalues that are nearly zero. It is probable that there is one unstable mode on the lower branch of solutions, as well as two unstable modes on the upper branch and two neutrally stable modes at the minimum Reynolds number solution.

6. Discussion. Nagata [5] finds new solutions to the equations for plane Couette flow. By using a different approximation scheme in a primitive variable formulation and path-following techniques, these solutions are confirmed. Two criticisms of these solutions have been raised by experimenters [7]. The first criticism is of the resolution of Nagata's solutions; however, these solutions exist at relatively high resolutions (see Table 5.1). The second criticism is a question about the stability of the solutions.

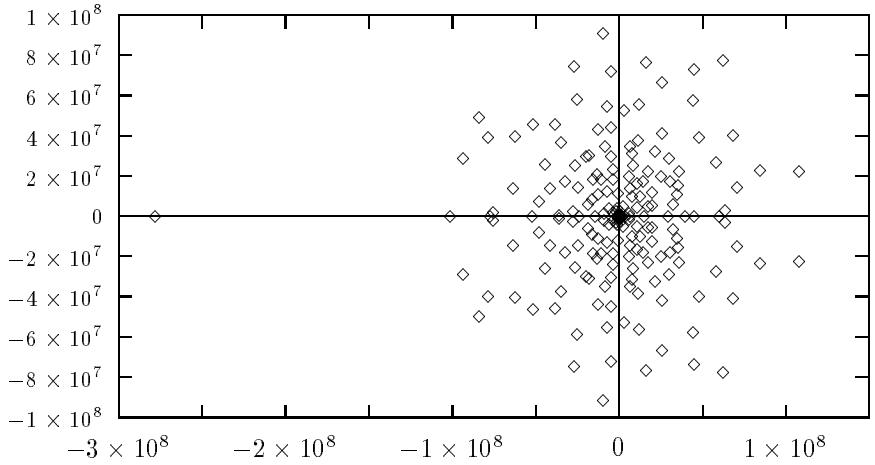

FIG. 5.5. *All the eigenvalues that we compute (including those perturbed from infinity) of the lower branch wavy vortex solution. We magnify the center of this graph by a factor of 100 to get the next figure.*

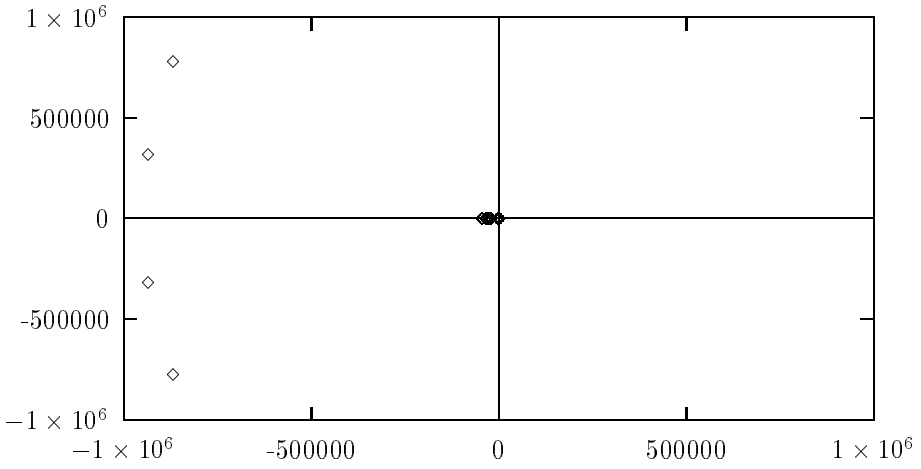

FIG. 5.6. *The eigenvalues near the origin of the previous figure. There are 588 eigenvalues clustered near the origin. This cluster of eigenvalues is shown (magnified) in the next figure.*

These solutions are not stable; however, there may be values of the parameters, Re, α_y, and α_z for which the solutions are stable (see Figures 5.7, 5.8, and 5.9). There are probably no wavy vortex solutions for Reynolds numbers less than 470.

The vortex branch of solutions bifurcates from and reconnects to the Couette flow branch (see Figure 4.6). This behavior indicates that in an experiment, as the Coriolis force is increased, Couette flow would bifurcate to vortices and the vortices would subsequently bifurcate back to Couette flow.

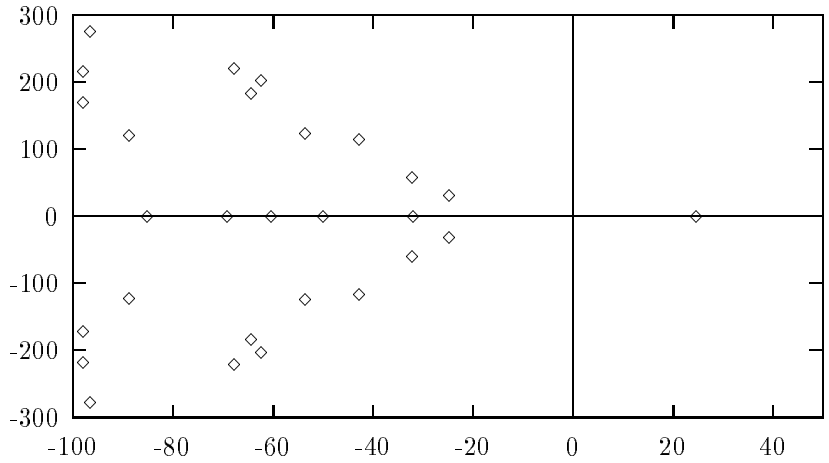

FIG. 5.7. *Eigenvalues of lower branch solution near the origin. Note the one unstable eigenvalue to the right of the imaginary axis. The parameter values are* $Re = 600, \alpha_y = 1.6, \alpha_z = 3.0, \tau = 1.7$.

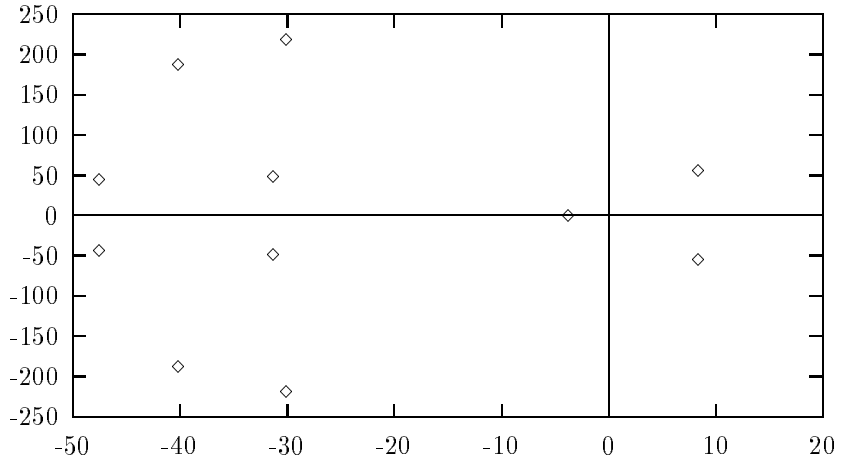

FIG. 5.8. *The eigenvalues of the upper branch solution has two unstable "Hopf pair" eigenvalues.*

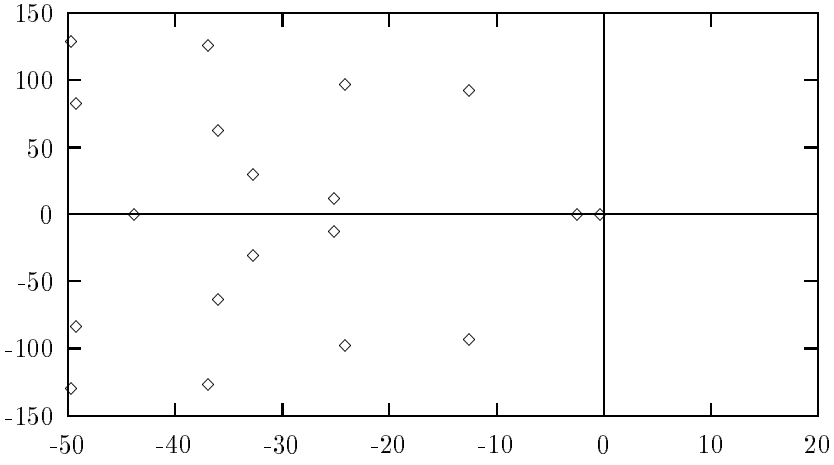

FIG. 5.9. *The eigenvalues nearest the origin for the solution at* $Re = 470, \alpha_y = 0.96, \alpha_z = 2.00$.

A. Relation of Taylor–Couette Flow and Couette Flow.

A.1. Taylor–Couette Flow. Taylor–Couette flow is the flow between concentric cylinders. If the gap width, a, between the cylinders is negligible compared with the average of the radii of the cylinders, b, then the equations governing Taylor–Couette flow are approximately the same as the equations for flow between parallel plates in a rotating frame.

The incompressible Navier–Stokes equations in cylindrical coordinates are

$$\frac{\partial V_\rho}{\partial \tau} + (\vec{V}\cdot\vec{\nabla})V_\rho - \frac{{V_\theta}^2}{\rho} = -\frac{\partial P}{\partial \rho} + \nu(\nabla^2 V_\rho - \frac{2}{\rho^2}\frac{\partial V_\theta}{\partial \theta} - \frac{V_\rho}{\rho^2}), \tag{A.1}$$

$$\frac{\partial V_\theta}{\partial \tau} + (\vec{V}\cdot\vec{\nabla})V_\theta + \frac{V_\rho V_\theta}{\rho} = -\frac{1}{\rho}\frac{\partial P}{\partial \theta} + \nu(\nabla^2 V_\theta + \frac{2}{\rho^2}\frac{\partial V_\rho}{\partial \theta} - \frac{V_\theta}{\rho^2}), \tag{A.2}$$

$$\frac{\partial V_\zeta}{\partial \tau} + (\vec{V}\cdot\vec{\nabla})V_\zeta = -\frac{\partial P}{\partial \zeta} + \nu(\nabla^2 V_\zeta), \tag{A.3}$$

$$0 = \vec{\nabla}\cdot\vec{V} = \frac{1}{\rho}(\frac{\partial}{\partial \rho}(\rho V_\rho)) + \frac{1}{\rho}(\frac{\partial V_\theta}{\partial \theta}) + \frac{\partial V_\zeta}{\partial \zeta}, \tag{A.4}$$

where

$$\vec{V}\cdot\vec{\nabla} = V_\rho\frac{\partial}{\partial \rho} + \frac{V_\theta}{\rho}\frac{\partial}{\partial \theta} + V_\zeta\frac{\partial}{\partial \zeta},$$

$$\nabla^2 = \frac{1}{\rho}\frac{\partial}{\partial \rho}(\rho\frac{\partial}{\partial \rho}) + \frac{1}{\rho^2}\frac{\partial^2}{\partial \theta^2} + \frac{\partial^2}{\partial {\zeta}^2}.$$

The domain is

$$\rho \in [R_0, R_1],\ \theta \in [-\infty, \infty],\ \zeta \in [-\infty, \infty],$$

and boundary conditions are

$$\vec{V}(R_0, \theta, \zeta, \tau) = V_0\hat{\theta}, \vec{V}(R_1, \theta, \zeta, \tau) = V_1\hat{\theta}, \tag{A.5}$$

where $\hat{\theta}$ is the unit vector in the θ direction.

A.2. Change of Variables. Use the width of the gap, a, between the cylinders to scale the lengths in the problem. Scale the time by a^2/ν. The velocity scale ($\bar{V}$) is chosen later. Use a reference frame that rotates with the average rotation rate, ω, of the cylinders. Explicitly, the change of variables is as follows:

$$\omega = \frac{V_1 + V_0}{2b},$$

$$b = \frac{R_1 + R_0}{2}, a = R_1 - R_0,$$

$$x = \frac{\rho - b}{a}, y = \frac{b(\theta - \omega\tau)}{a}, z = \frac{\zeta}{a},$$

$$t = \frac{\nu\tau}{a^2},$$

$$\bar{V}\,\vec{u}(x, y, z, t) = \vec{V}(\rho, \theta, \zeta, \tau) - \rho\omega\hat{\theta},$$

$$\frac{\nu \bar{V}}{a} p = P - \frac{\omega^2}{2}\rho^2,$$

where

$$\vec{V} = \begin{pmatrix} V_\rho \\ V_\theta \\ V_\zeta \end{pmatrix}, \vec{u} = \begin{pmatrix} u \\ v \\ w \end{pmatrix}.$$

The Navier–Stokes equations become

$$\begin{aligned} u_t = &-\mathrm{Re}\left[(\vec{u}\cdot\vec{\nabla})u - \frac{\epsilon v^2}{1+\epsilon x}\right] + 2\Omega v - \frac{\partial p}{\partial x} \\ &+(\nabla^2 u - \frac{2\epsilon}{(1+\epsilon x)^2}\frac{\partial v}{\partial y} - \frac{\epsilon^2}{(1+\epsilon x)^2}u), \end{aligned} \tag{A.6}$$

$$\begin{aligned} v_t = &-\mathrm{Re}\left[(\vec{u}\cdot\vec{\nabla})v + \frac{\epsilon u v}{1+\epsilon x}\right] - 2\Omega u - \frac{1}{1+\epsilon x}\frac{\partial p}{\partial y} \\ &+(\nabla^2 v + \frac{2\epsilon}{(1+\epsilon x)^2}\frac{\partial u}{\partial y} - \frac{\epsilon^2}{(1+\epsilon x)^2}v), \end{aligned} \tag{A.7}$$

$$\begin{aligned} w_t = &-\mathrm{Re}\left[(\vec{u}\cdot\vec{\nabla})w\right] - \frac{\partial p}{\partial z} \\ &+(\nabla^2 w), \end{aligned} \tag{A.8}$$

$$0 = \vec{\nabla}\cdot\vec{u} = \frac{\partial u}{\partial x} + \frac{\epsilon}{1+\epsilon x}u + \frac{1}{1+\epsilon x}\frac{\partial v}{\partial y} + \frac{\partial w}{\partial z}, \tag{A.9}$$

where

$$\vec{u}\cdot\vec{\nabla} = u\frac{\partial}{\partial x} + \left(\frac{1}{1+\epsilon x}\right)v\frac{\partial}{\partial y} + w\frac{\partial}{\partial z},$$

$$\nabla^2 = \frac{\partial^2}{\partial x^2} + \frac{1}{(1+\epsilon x)^2}\frac{\partial^2}{\partial y^2} + \frac{\partial^2}{\partial z^2} + \frac{\epsilon}{1+\epsilon x}\frac{\partial}{\partial x},$$

$$\epsilon = \frac{a}{b}, \quad \Omega = \frac{a^2}{\nu}\omega, \quad \mathrm{Re} = \frac{\bar{V}a}{\nu},$$

$$x \in [-1/2, 1/2], y \in [-\infty, \infty], z \in [-\infty, \infty].$$

The boundary conditions are the following:

$$u(\pm 1/2, y, z, t) = 0, \tag{A.10}$$

$$v(\pm 1/2, y, z, t) = \pm\frac{1}{2}\left(\frac{V_1 - V_0}{\bar{V}}\right) \mp \frac{\Omega}{2\mathrm{Re}}, \tag{A.11}$$

$$w(\pm 1/2, y, z, t) = 0. \tag{A.12}$$

A.3. Thin–Gap Limit. In the limit $\epsilon \to 0$, these equations reduce to the Cartesian equations satisfied by a fluid between parallel plates in a rotating frame:

$$\vec{u}_t = -\mathrm{Re}(\vec{u}\cdot\vec{\nabla})\vec{u} - 2\Omega(\hat{z}\times\vec{u}) - \vec{\nabla}p + \nabla^2\vec{u}, \tag{A.13}$$

$$0 = \vec{\nabla}\cdot\vec{u}. \tag{A.14}$$

The rotation, Ω, is about the z axis which is the axis of rotation of the cylinders. The boundary conditions are the following:

(A.15) $$u(\pm 1/2, y, z, t) = 0,$$

(A.16) $$v(\pm 1/2, y, z, t) = \pm\frac{1}{2}\left(\frac{V_1 - V_0}{\bar{V}}\right) \mp \frac{\Omega}{2\mathrm{Re}},$$

(A.17) $$w(\pm 1/2, y, z, t) = 0.$$

When

$$\Omega = 0, \bar{V} = V_1 - V_0,$$

the equations are satisfied by plane Couette flow.

B. Derivation of the Taylor number. Start with the Navier–Stokes equations linearized about a shear flow $(\vec{V}, p)$; that is, seek flows of the form $(\vec{V} + \vec{\epsilon}, p + \rho)$, where $\vec{V}$ varies only with x and $\vec{\epsilon}$ is "small." Dropping quadratic terms in $\vec{\epsilon}$ leads to the following:

(B.1) $$0 = -\mathrm{Re}((\vec{V} \cdot \vec{\nabla})\vec{\epsilon} + (\vec{\epsilon} \cdot \vec{\nabla})\vec{V}) - 2\Omega(\hat{z} \times \vec{\epsilon}) - \vec{\nabla}\rho + \nabla^2\vec{\epsilon},$$

(B.2) $$0 = \vec{\nabla} \cdot \vec{\epsilon},$$

where

(B.3) $$\vec{\epsilon}(\pm 1/2, y, z) = 0.$$

Seeking solutions in the form

$$\vec{\epsilon} = \begin{pmatrix} \epsilon_x(x)\cos(\alpha z), \\ \epsilon_y(x)\cos(\alpha z) \\ \epsilon_z(x)\sin(\alpha z) \end{pmatrix},$$

$$\rho = \rho(x)\cos(\alpha z),$$

$$\vec{V} = x\hat{y}.$$

with Eqs. (B.1)–(B.3) implies

$$\begin{aligned} \epsilon_z &= -\frac{1}{\alpha}\frac{\partial \epsilon_x}{\partial x}, \\ \epsilon_y &= -\frac{1}{2\Omega\alpha^2}(\frac{\partial^2}{\partial x^2} - \alpha^2)\epsilon_x, \\ \rho &= \frac{1}{\alpha^2}(\frac{\partial^2}{\partial x^2} - \alpha^2)\frac{\partial \epsilon_x}{\partial x}. \end{aligned}$$

Then ϵ_x must satisfy the linear eigenvalue problem

(B.4) $$0 = T\alpha^2\epsilon_x + (\frac{\partial^2}{\partial x^2} - \alpha^2)^3\epsilon_x,$$

(B.5) $$\epsilon_x(\pm 1/2) = \frac{\partial}{\partial x}(\epsilon_x)(\pm 1/2) = (\frac{\partial^2}{\partial x^2} - \alpha^2)^2(\epsilon_x)(\pm 1/2) = 0,$$

where

(B.6) $$T = 2\Omega(\mathrm{Re} - 2\Omega).$$

REFERENCES

[1] P. G. Drazin and W. H. Reid, *Hydrodynamic Stability*, Cambridge University Press, 1981.

[2] H. B. Keller, *Numerical Methods in Bifurcation Problems*, Springer-Verlag, 1987.

[3] M. Nagata, *Bifurcations in Couette flow between almost corotating cylinders*, J. Fluid Mech., 169 (1986), pp. 229–250.

[4] ———, *On wavy instabilities of the Taylor-vortex flow between corotating cylinders*, J. Fluid Mech., 188 (1988), pp. 585–598.

[5] ———, *Three-dimensional finite-amplitude solutions in plane Couette flow: Bifurcation from infinity*, J. Fluid Mech., 217 (1990), pp. 229–250.

[6] V. A. Romanov, *Stability of plane parallel Couette flow*, Functional Anal. and Its Applics., 7 (1973), pp. 137–146.

[7] N. Tillmark and P. H. Alfredsson, *Experiments on transition in plane Couette flow*, J. Fluid Mech., 235 (1992), pp. 89–102.